ICARUS 118 373–383 (1995)

Basalt Oxidation and the Formation of Hematite on the Surface of Venus

B. FEGLEY, JR.

Department of Earth and Planetary Sciences, Campus Box 1169, Washington University, One Brookings Drive, St. Louis, Missouri 63130-4899
E-mail: bfegley@planet.win.net

G. KLINGELHÖFER

Institut für Kernphysik, Technische Hochschule Darmstadt, Schlossgartenstrasse 9, D64289 Darmstadt, Germany

AND

R. A. BRACKETT, N. IZENBERG, D. T. KREMSER, AND K. LODDERS

Department of Earth and Planetary Sciences, Campus Box 1169, Washington University, One Brookings Drive, St. Louis, Missouri 63130-4899

Received March 15, 1995; revised July 10, 1995

We present experimental results showing that basalt is oxidized in gas mixtures with CO number densities approximately equal to those at the surface of Venus. Although the gas mixtures have CO/CO_2 ratios falling inside the magnetite stability field, Mössbauer spectroscopy shows that hematite and Fe^{3+} in pyroxene are produced in the oxidized basalt. The results suggest that the red color observed at several Venera landing sites is due to sub-aerial oxidation of Fe^{2+}-bearing basalt on the surface of Venus, and that hematite, instead of magnetite, is present on the surface of Venus.

INTRODUCTION

The global mean surface temperature of Venus is about 740 K and the global mean pressure is about 95 bars, dominated by CO_2 (~96.5%) and N_2 (~3.5%), with trace amounts of CO and other reactive gases (e.g., H_2O, SO_2, OCS, HCl, HF). The massive CO_2 atmosphere and the presence of reactive gases such as SO_2, OCS, HCl, and HF are direct consequences of the high surface temperature of Venus (e.g., see Fegley and Treiman 1992). Likewise, it is generally believed that the oxidation state of the surface of Venus is controlled by thermochemical gas–solid reactions such as

$$CO_2(g) + 2Fe_3O_4(\text{magnetite}) = CO(g) + 3Fe_2O_3(\text{hematite}), \quad (1)$$

with CO_2, the dominant atmospheric constituent (e.g., Mueller 1964; Lewis 1970; Prinn 1985; Fegley and Treiman 1992). The equilibrium CO/CO_2 ratios, and hence the equilibrium oxygen fugacities for reaction (1) and for the analogous reactions involving pyroxene and olivine,

$$CO_2(g) + 2FeSiO_3(\text{ferrosilite in pyroxene}) = Fe_2O_3(\textit{hematite}) + 2SiO_2(\textit{silica}) + CO(g) \quad (2)$$

$$CO_2(g) + Fe_2SiO_4(\text{fayalite in olivine}) = Fe_2O_3(\text{hematite}) + SiO_2(\text{silica}) + CO(g), \quad (3)$$

are independent of the total pressure because reactions (1)–(3) have the same number of gas molecules (one) on each side of the equations. Thus, total pressure cancels out of the equilibrium constant expressions, which then depend only on the temperature.

In-situ measurements by the Pioneer Venus spaceprobe show that the CO mixing ratio in the lower atmosphere of Venus varies from 30 ± 18 ppm at 42 km to 20 ± 3 ppm at 22 km altitude (Von Zahn *et al.* 1983). A similar trend in this altitude region was deduced from Earth-based IR observations of the nightside of Venus by Pollack *et al.* (1993). However, the CO abundance below 22 km altitude in the atmosphere of Venus is not well constrained. *In situ* measurements of the CO abundance by the Pioneer Venus spacecraft at 22 km of 20 ± 3 ppm (Von Zahn *et al.* 1983) and by the Venera 11/12 spacecraft at 12 km of 17 ± 1 ppm (Gel'man *et al.* 1979; Marov *et al.* 1989) are the same within the measurement uncertainties. As discussed elsewhere (e.g., by Fegley *et al.* 1992), the measured CO/CO_2

0019-1035/95 $12.00

ratios of ~18–21 ppm lie inside the magnetite stability field at Venus surface temperatures and thus hematite is predicted to be thermodynamically unstable on the surface of Venus. (Note that because CO_2 comprises 96.5% of the atmosphere of Venus the CO/CO_2 ratio is equal to 1/0.965 times the CO mixing ratio.)

Unfortunately no direct measurements of either the mineralogy of the surface of Venus or of the chemical composition of the lower 12 km of the atmosphere of Venus are available to test the predictions of the thermochemical equilibrium models. Two indirect, apparently contradictory observations of the oxidation state of the lower atmosphere and surface of Venus do, however, exist. Pieters *et al.* (1986) used a combination of the Venera 9/10 wide angle photometer measurements and the Venera 13/14 color images to derive the spectral reflectance of the venusian surface in the range 0.54 to 1.0 μm. They found that at visible wavelengths the spectral reflectance of the venusian surface was not diagnostic about the Fe oxidation state (with either Fe^{2+}- or Fe^{3+}-bearing minerals being acceptable), but that a high reflectance in the near-IR region apparently required Fe^{3+}-bearing phases such as hematite.

The second indirect observation comes from the CONTRAST experiment on the Venera 13/14 landers, which qualitatively measured the oxygen fugacity at the surface of Venus from the color change from white to blue for the reaction

$$Na_4V_2O_7 + CO_2 + CO = V_2O_4 + 2Na_2CO_3 \quad (4)$$

or from white to black for the reaction

$$Na_4V_2O_7 + 2CO = V_2O_3 + 2Na_2CO_3 \quad (5)$$

for asbestos paper impregnated with sodium pyrovanadate ($Na_4V_2O_7$). The observed darkening of the asbestos paper (Florensky *et al.* 1983) gave a lower limit of $\geq$10 ppm for the CO mixing ratio and an upper limit of $\leq 10^{-21}$ atm for the oxygen fugacity. The deduced CO mixing ratio is consistent with the value of 17 $\pm$ 1 ppm measured by the Venera 11/12 gas chromatograph at 12 km altitude (Gel'man *et al.* 1979; Marov *et al.* 1989) and the deduced oxygen fugacity is inside the magnetite stability field at Venus surface temperatures. However, darkening of the asbestos paper by dust thrown up by the spacecraft landing could not be ruled out, so the results of this experiment may be somewhat subjective.

Prior experimental work has demonstrated that atmosphere-surface reactions of sulfur gases on Venus, such as SO_2 loss by anhydrite formation and reduced sulfur gas production by pyrite decomposition, are kinetically controlled (Fegley and Prinn 1989, Fegley *et al.* 1995). We therefore decided to experimentally study whether or not redox reactions between Fe-bearing phases and CO–CO_2 gas mixtures may also be kinetically controlled.

Below we report experimental data showing that hematite and Fe^{3+} in pyroxene are formed by heating basalt samples in gas mixtures with CO/CO_2 ratios inside the magnetite stability field. We also report results from experiments with synthetic Fe_3O_4 and CuO showing that CO–CO_2 gas mixtures do not thermochemically equilibrate at Venus surface temperatures. Instead we find that while still highly reducing, the oxygen fugacities of CO–CO_2 gas mixtures (at Venus surface temperatures) are several orders of magnitude more oxidizing than predicted by thermochemical equilibrium calculations using JANAF data. Preliminary descriptions of this work were given by Fegley *et al.* (1994a, 1994b).

EXPERIMENTAL METHODS

Well-characterized, powdered tholeiitic basalt from the Vogelsberg region of Germany was used in the experiments for two reasons: (i) geologic interpretation of Magellan radar observations shows that the majority of landforms are consistent with basaltic compositions (e.g., Head *et al.* 1992), and (ii) most of the elemental analyses by gamma ray spectroscopy and X-ray fluorescence at several Venera and Vega landing sites are consistent with tholeiitic basalt compositions (e.g., Kargel *et al.* 1993 and references therein).

The chemical composition of the basalt powder used was analyzed by X-ray fluorescence spectroscopy and instrumental neutron activation analysis at the Max Planck Institut für Chemie, Mainz, Germany (Lodders 1991) and the mineralogy of the basalt was determined by powder X-ray diffraction, optical microscopy, energy dispersive spectroscopy, and electron microprobe analyses at Washington University, and for Fe-bearing phases by Mössbauer (MB) spectroscopy (at the Institut für Kernphysik of the Technische Hochschule, Darmstadt, Germany). The X-ray diffraction patterns were taken on a Rigaku powder diffractometer with Cu$K\alpha$ radiation and calibrated with an external Si standard (NIST). The electron microprobe analyses (see Table I) were done using a JEOL-733 electron microprobe equipped with Advanced Microbeam automation. The accelerating voltage, beam current, and beam diameter were 15 kV, 20–30 nA, and 1–10 μm, respectively. Simple oxides and minerals were used as primary standards and X-ray matrix corrections were based on a modified Armstrong (1988) CITZAF routine incorporated into the software. The energy dispersive spectroscopy was also done using the Washington University electron microprobe.

The Mössbauer spectra of the unreacted basalt and run products were measured in transmission geometry at room temperature. The experimental setup consists of a loud-

TABLE I
Chemical Composition (wt%) of Basalt Used in the Experiments

Component	Basalt powder[a]	Olivine[b]	Pyroxene[b]	Feldspar[b]
SiO_2	49.59	39.35	47.89	56.19
TiO_2	2.37	<0.03	2.65	na
Al_2O_3	11.69	<0.02	5.83	27.20
FeO[c]	10.22	19.83	6.63	0.65
MnO	0.15	0.33	0.12	na
MgO	11.67	40.23	13.51	na
CaO	8.76	0.32	22.39	9.21
Cr_2O_3	0.07	<0.04	0.31	na
Na_2O	2.43	<0.03	0.47	5.41
K_2O	1.64	<0.01	<0.01	0.94
Sum	98.59	100.06	99.80	99.86[d]

Note. na, not analyzed.
[a] From Lodders (1991).
[b] Electron microprobe analyses which are averages of 6, 5, and 7 analyses, respectively, for the olivine, pyroxene, and feldspar.
[c] All Fe is reported as FeO.
[d] Includes 0.26% BaO.

speaker-type drive, developed at Darmstadt (Kankeleit 1964, 1975), running in constant acceleration mode, and a Si PIN diode (Klingelhöfer *et al.* 1995, Kankeleit *et al.* 1994) for the detection of the 14.4-keV Mössbauer radiation. A ^{57}Co/Rh Mössbauer source with an activity of ~200 mCi was used, having a linewidth of ~0.2 mm sec^{-1}. The typical absorber thickness used for the measurements was about 25 mg cm^{-2} and thickness effects can be assumed to be small. Recording times for one spectrum are about 1–4 days. All isomer shift values in this paper are reported relative to α-Fe. The Mössbauer spectra were analyzed assuming a Voigt lineshape (convolution of Lorentzian and Gaussian line profiles) for the resonance lines.

Two sets of heating experiments were done. In one set, basalt powder samples weighing several hundred milligrams were isothermally heated in alumina crucibles in flowing CO–CO_2 gas mixtures at ambient pressure in Deltech vertical tube furnaces for several days. In the second set, synthetic magnetite and CuO (both 99.999%, Johnson Matthey Puratronic grade) were heated under the same conditions. The experimental protocols are summarized in Table II. The gas mixtures used in all the experiments are certified standards prepared by the commercial supplier. The CO concentrations in the certified standard gas mixtures are accurate to ±2% of the stated value. The mixtures in the basalt oxidation experiments contained 1000 parts per million by volume (ppm) CO, while those used in the metal oxide experiments contained from 100 to ~37,000 ppm CO. The CO molecular number density in the basalt oxidation experiments was thus about 50% of that at the surface of Venus, while the CO molecular number densities in the metal oxide experiments ranged from about 0.05–20 times that at the surface of Venus. After cooling in the CO–CO_2 gas mixtures inside the top of the furnaces, which took <5 min, the basalt and metal oxide samples were removed, weighed, and characterized by powder X-ray diffraction at Washington University. The unreacted and reacted basalt samples were also analyzed by Mössbauer spectroscopy as described above.

We ruled out the possibility of reactions taking place during the heating and cooling of samples by heating some basalt powder in air at ~110° C in a drying oven for a few days. The powder was analyzed by MB spectroscopy before and after this heating. There is no change in the MB spectra after this heating. The heating in the drying oven was much longer (days vs minutes) than the time the samples spend heating and cooling. Thus no reactions take place in our samples during insertion into or removal from the furnace. This experiment also shows that any adsorbed water and oxygen in the samples are unimportant for basalt oxidation because the identical MB spectra before and after heating show that no oxidation took place during these experiments.

EXPERIMENTAL RESULTS

(*a*) *Unreacted Basalt*

The basalt mineralogy as determined by XRD, optical microscopy, energy dispersive spectroscopy, and electron microprobe analysis is dominantly plagioclase feldspar ($Ab_{46}An_{50}Or_4$) and clinopyroxene ($Wo_{49}En_{40}Fs_{11}$) with smaller amounts of olivine ($Fo_{78}Fa_{22}$) and trace ilmenite. We carefully looked for but did not find any glass in the basalt starting material. We also carefully looked for but did not find any trace Fe-bearing phases other than ilmenite in the basalt. The two major Fe-bearing phases are olivine and clinopyroxene. Ilmenite and feldspar contain minor amounts of the total Fe in the basalt. Representative analyses for the major minerals are given in Table I. The composition and mineralogy are in good agreement with analyses of other tholeiites from the Vogelsberg region (e.g., Kreuzer *et al.* 1974, Ehrenberg *et al.* 1982).

These results are consistent with those obtained by Mössbauer spectroscopy. Figure 1 shows the Mössbauer spectrum for the unreacted basalt sample. The corresponding MB parameters and the relative intensities of the different Fe-bearing phases in the samples are summarized in Table III. A reasonably good statistical fit with a normalized χ^2 value of 1.25 for the MB data of the unreacted basalt was obtained by using at least four doublets (quadrupole split components). The best fit (χ^2 = 1.17) was obtained using five quadrupole split doublets, but no statistically significant improvement (within the statistical variation of the χ^2 value) of the fit results was observed

TABLE II
Experimental Runs

Run no.	Temp. (°C)	Time (days)	CO (ppm)[a]	$\log_{10} f_{O2}$ (atm) Predicted[b]	$\log_{10} f_{O2}$ (atm) Observed[c]	Starting material	Final product(s)[d]
			Basalt oxidation experiments in $CO-CO_2$				
ZT1	505	7	1,000	−22.9	≥−19.0	Basalt	See Table III
BBB1	803	10	1,000	−12.3	>−9.4	Basalt	See Table III
			Metal oxide experiments				
R118	417	3.8	100	−25.7	≥−23.4	Fe_3O_4	$Fe_3O_4 + Fe_2O_3$
R132	392	4.8	10,100	−31.4	≥−24.9	Fe_3O_4	$Fe_3O_4 + Fe_2O_3$
R133	415	1	10,100	−29.9	<−14.1	CuO	Cu metal
R136	415	1.8	10,100	−29.9	≥−23.5	Fe_3O_4	$Fe_3O_4 + Fe_2O_3$
R180	598	6.8	34,700	−21.9	<−9.3	CuO	Cu metal
R181	602	4.7	37,000	−21.8	≤−15.2	Fe_2O_3	$Fe_3O_4 + Fe_2O_3$

[a] Carbon dioxide makes up the balance of the gas mixture. All gases are certified standard gas mixtures from a commercial supplier.

[b] The oxygen fugacity (atm) predicted from the CO/CO_2 ratio of the gas mixture and thermodynamic data from the JANAF Tables (Chase *et al.* 1985) is given by the equation:

$$\log_{10} f_{O_2} = 2 \log_{10} (X_{CO_2}/X_{CO}) + 9.170 - 29607.34/T,$$

where X_i is the mixing ratio of gas i and T is temperature in Kelvin.

[c] The observed f_{O_2} is deduced from the composition of the final products. Magnetite + hematite shows an oxygen fugacity at or above the magnetite/hematite boundary, hematite alone shows an oxygen fugacity above the magnetite/hematite boundary, and Cu metal alone shows an oxygen fugacity below the CuO/Cu boundary.

[d] The temperature-dependent oxygen fugacity for the Cu/CuO and Fe_3O_4/Fe_2O_3 phase boundaries are given Eqs. (9) and (11) in the text.

by using more than five quadrupole split doublets or magnetically split sextets as, for instance, a magnetite component. From these fits the amount of magnetite in the unreacted basalt was determined to be ~0–0.2 wt%, with an upper limit of <0.4 wt% giving the same χ^2 value. In the present case, MB spectroscopy is very sensitive to magnetite and hematite because the corresponding sextets are clearly resolved from the silicate doublets (see Fig. 2), and because of the high iron content per mole of hematite and magnetite (e.g., see the relative intensity versus relative mass given in Table III for samples ZT1 and BBB1, respectively).

As shown in Fig. 1 and Table III, the five different MB doublets could be attributed to the following Fe components: ilmenite, which contains Fe^{2+}, olivine, which contains Fe^{2+}, and clinopyroxene (augite), which contains Fe^{2+} in M1 (almost perfect octahedral symmetry) and M2 (highly distorted octahedral symmetry approximated as C_{2v} symmetry) sites, and Fe^{3+}. The M1 component having a larger quadrupole splitting than the M2 component indeed has a significantly smaller linewidth than the M2 site. This is expected because the lattice site distortions in the M2 site result in line broadening.

The Fe^{3+} component in the MB spectrum was attributed to pyroxene and not to olivine for two reasons. First, the isomer shift and quadrupole splitting are consistent with Fe^{3+} in M1 pyroxene sites (Burns 1994). Second, X-ray diffraction did not detect olivine, although optical microscopy, energy dispersive spectroscopy, and electron microprobe analysis show that olivine is present in small amounts (less than a few percent).

The trace amounts of Fe present in the feldspar were not determined from the MB spectra. As illustrated in Fig. 1 and Table III, the MB spectrum of the unreacted basalt is dominated by Fe^{2+} in augite, with Fe^{3+} in the augite being the second most abundant component, Fe^{2+} in olivine coming next, and Fe^{2+} in ilmenite being the least abundant component. Based on the present work and on our prior use of MB spectroscopy to detect magnetite and hematite in our pyrite decomposition experiments (Fegley *et al.* 1995) we know that MB spectroscopy can detect as little as 0.4% magnetite. Thus, we are confident that no other trace Fe-bearing phases other than ilmenite are present in the basalt starting material.

(*b*) *Oxidized Basalts*

As illustrated in Fig. 2 and Table III, the MB spectra systematically change in going from the unheated powder to sample ZT1 (505°C for 7 days) to sample BBB1 (803°

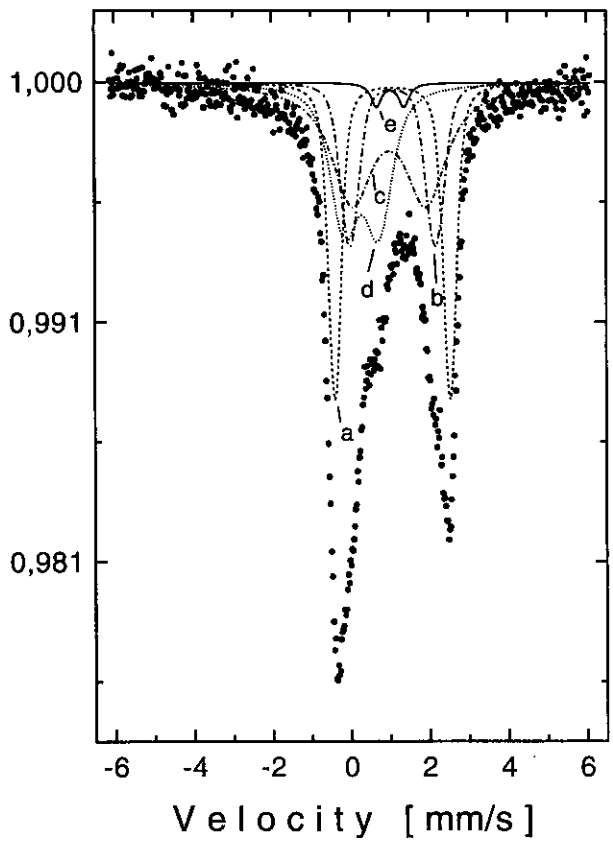

FIG. 1. The MB spectrum of the unreacted basalt. Components are assigned as follows: (a) olivine, (b) pyroxene M1 site, (c) pyroxene M2 site, (d) Fe^{3+} in pyroxene, (e) ilmenite.

C for 10 days). The changes are due to the decreasing amount of Fe^{2+} and to the increasing amount of Fe^{3+} in the basalt samples. The evolution of the MB spectra also correlates with increased reddening in the samples from gray (starting material) to rose (ZT1) to reddish (BBB1).

After sample ZT1 is heated at about 500° C for 7 days, the amounts of Fe^{2+} in olivine and clinopyroxene have decreased, the amount of Fe^{3+} in clinopyroxene has increased, and magnetite and hematite have been formed. The magnetite is close to, but not exactly, stoichiometric with a B/A ratio of ~1.9. The larger linewidth found for the B site component (Fe^{2+} and Fe^{3+} in octahedral sites) is due to electron hopping between Fe^{2+} and Fe^{3+} (Sawatzky *et al.* 1969, Mitra 1992). The hematite component was fitted with one sextet having magnetic hyperfine parameters and a quadrupole distortion nearly identical to bulk hematite. This high magnetic hyperfine field of 51.6 T, which is very close to the maximum value observed for pure bulk hematite, and the absence of any asymmetry in the lineshape indicate the presence of well crystallized and relatively large hematite particles with very little (if any) substitution of Fe by Al (see the description for BBB1 below).

More intense heating at about 800° C for 10 days (sample BBB1) leads to further decreases in the amounts of Fe^{2+} in olivine and clinopyroxene, further increases in the amount of Fe^{3+} in clinopyroxene, a decrease below detection limit in the amount of magnetite, and an increase in the amount of hematite. Formation of vacancies in the pyroxene or formation of other phases from the pyroxene are both possible mechanisms to provide iron for the formation of magnetite and hematite while preserving mass balance.

As can be seen in Fig. 2, the lineshape of the hematite component is asymmetric in the MB spectrum for sample BBB1. A set of four different magnetically split sextets was needed to reproduce the data. The quadrupole distortion

TABLE III
Mössbauer Parameters for Unreacted and Oxidized Basalts

	Component	Isomer shift (mm sec^{-1})	Q.S. (mm sec^{-1}) or H.F. (T)[a]	Relative intensity (%)[b]	Relative mass (%)
		Unreacted Basalt			
A	Olivine Fe^{2+}	1.15	2.94 mm sec^{-1}	23.5	10.5
B	Cpx Fe^{3+}	0.37	0.88	28.2	31.0
C	Cpx Fe^{2+} (M1)	1.11	2.25	25.0	33.0
D	Cpx Fe^{2+} (M2)	1.05	1.80	22.0	25.0
E	Ilmenite Fe^{2+}	1.11	0.71	1.3	0.5
		Oxidized basalt ZT1			
A	Olivine Fe^{2+}	1.12	2.94	22.0	14.0
B	Cpx Fe^{3+}	0.37	0.95	34.0	51.0
C	Cpx Fe^{2+} (M1)	1.04	2.35	10.6	23.0
D	Cpx Fe^{2+} (M2)	1.12	1.85	4.9	8.0
E	Ilmenite Fe^{2+}	1.11	0.68	5.0	1.1
F	Hematite	0.37	51.6 T	3.5	0.5
G	Fe_3O_4 A site	0.26	48.3 T	7.0	0.8
	Fe_3O_4 B site	0.63	45.7 T	13.0	1.6
		Oxidized basalt BBB1			
A	Olivine Fe^{2+}	1.12	2.95	6.3	4.2
B	Cpx Fe^{3+}	0.36	0.87	41.0	63.3
C	Cpx Fe^{2+} (M1)	1.14	2.16	12.4	23.3
D	Cpx Fe^{2+} (M2)	1.13	1.90	3.0	5
E	Ilmenite Fe^{2+}	1.08	0.71	0.4	0.2
F	Hematite	0.36	49.76 T	10.8	1.2
		0.378	51.43 T	11.3	1.3
		0.37	43.64 T	8.5	1.0
		0.38	47.52 T	6.3	0.8

[a] Q.S., Quadrupole shift (mm sec^{-1}) and H.F., hyperfine splitting in T. Hyperfine splittings are listed for hematite and magnetite and quadrupole splittings are listed for the other components.

[b] The apparent variation in the ilmenite content, which is constant, gives an indication of the typical uncertainty in the relative intensities of strongly overlapping components. The typical uncertainty in the relative intensities of clearly resolved components, i.e., magnetite and hematite, is significantly smaller.

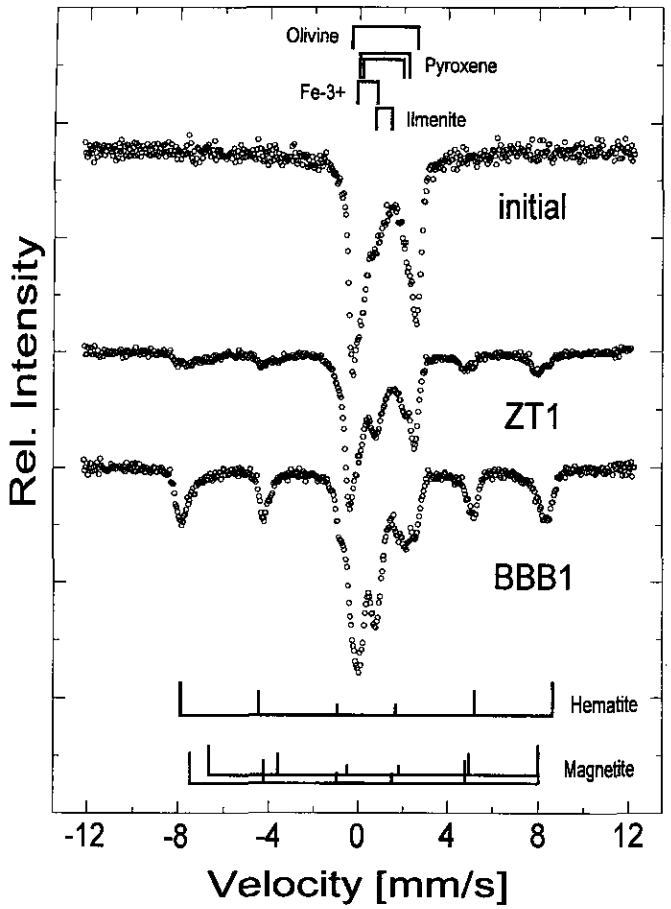

FIG. 2. A comparison of the MB spectra of the unreacted basalt and the two oxidized samples. The stick diagrams indicate the positions and relative intensities of the peaks for Fe^{2+} in olivine, Fe^{2+} in the M1 (outer) and M2 (inner) sites of clinopyroxene, Fe^{3+} in clinopyroxene, Fe^{2+} in ilmenite, Fe^{3+} in hematite and for the A (lower) and B (upper) sites of Fe_3O_4. Table III lists the MB parameters for the three spectra, which are described in the text.

determined for all four sextets is the same within error and matches well with the bulk hematite quadrupole splitting value of about -0.20 mm sec^{-1}. Other iron oxides such as maghemite and goethite have different quadrupole distortion or magnetic splitting values and can be excluded.

Two effects are responsible for the asymmetric lineshape and the reduction of the magnetic splitting of the hematite spectrum. A breakdown of the magnetic splitting, due to superparamagnetic relaxation, is observed for particles with small diameters on the order of a few nanometers (Kündig *et al.* 1966; van der Kraan 1973, Morris *et al.* 1989). Furthermore, the substitution of Fe by Al also causes a reduction of magnetic splitting values (Murad and Johnston 1987, Morris *et al.* 1992). Both effects may be present in this case and are difficult to distinguish. To evaluate from the data which effect might be dominant, one has to look for the quadrupole splitting values (QS). From systematic studies (Murad and Johnston 1987, Morris *et al.* 1992) it is known that QS shows no systematic variation with Al concentration, whereas for superparamagnetic particles (size on the order of a few nm up to about 20 nm) an increase of QS is found with decreasing particle size. For sample BBB1 all four sextets show a QS of about $-0.20(3)$, which is nearly identical with the bulk hematite value. This result is consistent with both a substitution of the Fe^{3+} in hematite by Al, and the presence of small hematite particles which are still large enough not to be superparamagnetic at room temperature. This question could be answered by an additional measurement taken at temperatures well below room temperature (e.g., at 77 K).

Finally, the amount of ilmenite in the unreacted basalt and in samples ZT1 and BBB1 is the same within uncertainty. The large variation in the amount of ilmenite detected is probably due to the low amount of this mineral and the large overlap of all components, leading to strong correlations between the fit results of the different components.

The growth of Fe^{3+} and the decrease of Fe^{2+} components in the basalt samples is summarized by the bar graphs in Fig. 3. These graphs show the relative intensities of Fe in olivine, pyroxene, ilmenite, magnetite, and hematite. These values, which are also listed in Table III, were converted into relative mass percentages by taking into account the different Debye–Waller factors for the different minerals (DeGrave and Van Alboom 1991, Fegley *et al.* 1995, Meisel *et al.* 1990).

(c) *Metal Oxide Experiments*

At thermochemical equilibrium, the oxygen fugacity of a CO–CO_2 gas mixture is controlled by the reaction

$$CO(g) + \tfrac{1}{2}O_2(g) = CO_2(g) \quad (6)$$

and is given by the equation

$$\log_{10} f_{O2} = 2\log_{10}(X_{CO_2}/X_{CO}) + 9.170 - 29607.34/T, \quad (7)$$

where X_i is the mixing ratio (or mole fraction) of gas i, T is the temperature in kelvins, and the coefficients are determined from thermodynamic data in the JANAF Tables (Chase *et al.* 1985).

Normally, we would use zirconia oxygen fugacity sensors to measure the oxygen fugacities of the gas mixtures in the experiments. However, zirconia sensors cannot be used in the present work because the experiments were done at temperatures below the operational range of these sensors, which is >700°C (Ceramic Oxide Fabricators Pty. Ltd. brochure). Thus, we used oxidation and reduction reac-

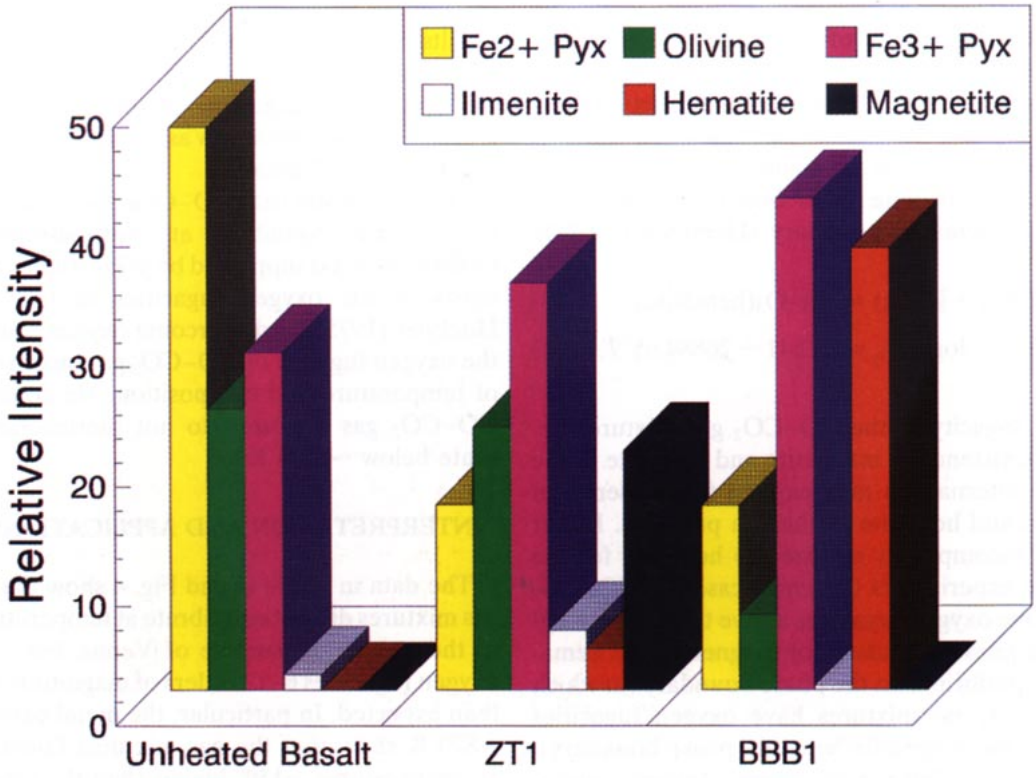

FIG. 3. The decreasing abundance of Fe^{2+} and the increasing abundance of Fe^{3+} in the unreacted basalt, ZT1, and BBB1. The relative intensities of Fe^{2+} and Fe^{3+} in the different minerals are plotted in the three sets of bar graphs.

tions of metal oxides to provide some qualitative constraints on the oxygen fugacities (f_{O_2}) of the CO–CO_2 gas mixtures used in the experiments.

We did one set of experiments by heating weighed samples of copper oxide powder (CuO) in several CO–CO_2 gas mixtures (listed in Table II). In experiment R133 the gas mixture was the same as that used in magnetite oxidation experiments R132 and R136. In another experiment (R180) the gas mixture was another tank from the same supplier and had almost the same CO/CO_2 ratio as the gas tank used in magnetite oxidation experiment R181. When the copper oxide powder was removed from the furnace after heating, it had quantitatively converted to copper metal. The quantitative conversion to Cu metal was verified by the X-ray diffraction pattern, which showed only Cu metal lines, and the observed weight loss, which corresponded to complete conversion of the original CuO powder to Cu metal. Thermodynamic data from the JANAF Tables (Chase *et al.* 1985) show that the CuO/Cu metal phase boundary

$$\mathrm{CuO(s)} = \mathrm{Cu(metal)} + \tfrac{1}{2}\mathrm{O_2(g)} \qquad (8)$$

corresponds to temperature-dependent oxygen fugacities (i.e., partial pressures) given by the equation:

$$\log_{10} f_{O_2} = 9.024 - 15942.24/T. \qquad (9)$$

Thus, the quantitative reduction of CuO to Cu metal proves that the oxygen fugacities inside the furnace were less than the oxygen fugacity of the CuO/Cu phase boundary (Eq. (9)) because no CuO was left in the sample. The two CuO reduction experiments listed in Table II were done at temperatures of 415°C (688 K) and 598°C (871 K) and atmospheric pressure. The upper limits to the oxygen abundances in the two experiments correspond to the CuO/Cu phase boundary (Eq. (9)) and are <0.000007 ppb (688 K) and <0.5 ppb (871 K). Thus, we are confident that there is no oxygen contamination in the compressed gases we are using and that there are no oxygen leaks in the furnaces we are using. Otherwise it would be impossible to reduce CuO to Cu metal as we have done in these two experiments.

We did an analogous set of experiments by heating synthetic magnetite powder in several CO–CO_2 gas mix-

tures (see Table II). The experiments done with magnetite always resulted in a mixture of magnetite plus hematite. This conversion was reflected by the color change (from black to reddish-black or red), the X-ray diffraction powder patterns, and the Mössbauer spectra (e.g., the MB spectrum shows that R118 is mainly hematite). These experiments set an absolute lower bound, corresponding to the magnetite/hematite boundary (Hemingway 1990)

$$2Fe_3O_4(\text{magnetite}) + \tfrac{1}{2}O_2(g) = 3Fe_2O_3(\text{hematite}) \quad (10)$$

$$\log_{10} f_{O_2} = 15.541 - 26884.65/T, \quad (11)$$

on the oxygen fugacity of the $CO-CO_2$ gas mixtures because of the coexistence of magnetite and hematite in the products. Two alternatives may explain the presence of both magnetite and hematite in the run products. Either magnetite was incompletely oxidized to hematite for the duration of the experiments (in which case the $CO-CO_2$ gas mixtures have oxygen fugacities above that of the magnetite/hematite phase boundary) or magnetite and hematite coexist in equilibrium on the phase boundary (in which case the $CO-CO_2$ gas mixtures have oxygen fugacities equal to that of the magnetite/hematite phase boundary). However, as shown in Table II, the observed oxygen fugacities of the $CO-CO_2$ gas mixtures, determined from the phase(s) in the products, were always several orders of magnitude more oxidizing than the oxygen fugacities predicted from the CO/CO_2 ratios of the mixtures and the experimental temperatures. Figure 4 summarizes the results of the two experiments done at 688 K (~8 km altitude on Venus) with the same $CO-CO_2$ gas mixture. These results bracket the "true" oxygen fugacity of a $CO-CO_2$ gas mixture containing ~1% CO and graphically illustrate that the oxygen fugacities of the gas mixtures, while extremely low, are not as low as predicted by thermochemical equilibrium calculations.

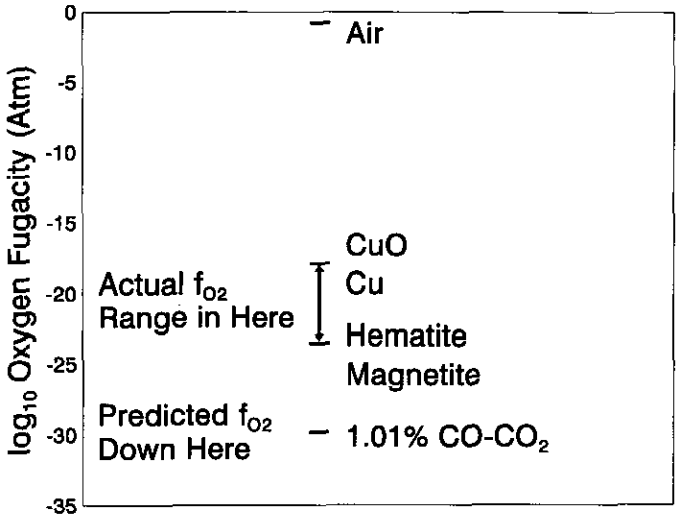

FIG. 4. A comparison of the predicted and observed oxygen fugacities in a $CO-CO_2$ gas mixture containing 1.01% CO at 416°C. The observed oxygen fugacity is between 6–12 orders of magnitude more oxidizing than predicted from thermochemical equilibrium calculations.

Our conclusion that $CO-CO_2$ gas mixtures do not thermochemically equilibrate at Venus surface temperatures (~660–740 K) is supported by prior studies done by petrologists of the oxygen fugacities of CO_2 gas mixtures. Huebner (1975) used a zirconia oxygen sensor to measure the oxygen fugacity of $CO-CO_2$ gas mixtures as a function of temperature and composition. He concluded that the $CO-CO_2$ gas mixtures do not thermochemically equilibrate below ~1373 K.

INTERPRETATION AND APPLICATIONS TO VENUS

The data in Table II and Fig. 4 show that the $CO-CO_2$ gas mixtures did not equilibrate at temperatures equivalent to those over the surface of Venus, but instead were at oxygen fugacities 6–12 orders of magnitude more oxidizing than expected. In particular, the metal oxide runs done at ~870 K show that the gas mixtures failed to equilibrate at temperatures ~130° higher than the global mean temperature in the plains of Venus and over 200° higher than the temperatures in the highest regions on Venus.

The production of hematite and Fe^{3+}-bearing pyroxene in the basalt oxidation experiments occurs because the basalt is reacting with gases that have an oxygen fugacity inside the stability fields of hematite and the Fe^{3+}-bearing pyroxenes. In other words, the failure of the $CO-CO_2$ gas mixtures to reach thermochemical equilibrium leads to a significantly more oxidizing environment that stabilizes Fe^{3+}-bearing phases at the expense of Fe^{2+}-bearing ones.

Our results show that basalt heated at Venus surface temperatures is oxidized in $CO-CO_2$ gas mixtures containing about the same number density (i.e., the same partial pressure) of CO as expected at the surface of Venus. Straub and Burns (1991) reported oxidation of pyroxene, but heated their samples in pure CO_2, in which production of hematite is predicted thermodynamically. They did not perform any experiments in $CO-CO_2$ gas mixtures. The red color observed by Pieters *et al.* (1986) at the Venera landing sites is plausibly due to hematite and other Fe^{3+}-bearing phases produced by the sub-aerial oxidation of erupted basalts. In other words, our experiments indicate that the near-surface environment on Venus is significantly more oxidizing than predicted on the basis of thermochemical equilibrium models of atmospheric chemistry.

By analogy with theoretical models of CO_2 photochemistry on Mars and Venus, and with experimental studies of combustion chemistry in the C/H/O system, we propose

that the CO and CO_2 in the near-surface atmosphere of Venus have not equilibrated because of the low water vapor abundance. The elementary reaction

$$CO + OH \rightarrow CO_2 + H \quad (12)$$

which has a rate constant (Mallard *et al.* 1994)

$$k_{12} = 2 \times 10^{-13}\,cm^3\,sec^{-1}, \quad (13)$$

is of basic importance for CO oxidation in flames and combustion processes (Warnatz 1984) and is also a key reaction in the catalytic cycles invoked for maintaining the CO_2 atmosphere of Mars (McElroy and Donahue 1972, Parkinson and Hunten 1972). Interestingly, reaction (12) is much less effective in the stratosphere of Venus than it is on Mars, due to the extremely low abundance of hydrogen compounds above the clouds of Venus (Yung and DeMore 1982). Apparently the anhydrous nature of the near-surface atmosphere of Venus (~20–30 ppm water vapor versus a few percent water vapor in the terrestrial troposphere) also inhibits reaction (12) and prevents the thermochemical equilibration of CO and CO_2 at the surface of Venus.

Prinn (1985) and later Krasnopolsky and Pollack (1994) discussed the reaction

$$CO + SO_3 \rightarrow CO_2 + SO_2 \quad (14)$$

as a part of the postulated fast atmospheric sulfur cycle on Venus. However, reaction (14) also provides a route for converting CO and CO_2. As noted by Krasnopolsky and Pollack (1994), no experimental rate data are available for reaction (14), but their models gave a rate constant of

$$k_{14} = 10^{-11} \exp(-13{,}100(\pm 1000)/T)\,cm^3\,sec^{-1}. \quad (15)$$

Thus, the ratio of the two rate constants (k_{12}/k_{14}) at a constant temperature is

$$(k_{12}/k_{14}) = 0.02 \exp(-13{,}100(\pm 1000)/T), \quad (16)$$

giving values of $\sim 10^{-9}$ (505° C) to $\sim 10^{-7}$ (803° C) over the temperature range of our basalt oxidation experiments. This calculation suggests that reaction (14) driven by SO_3 will be much less effective than reaction (12) driven by OH radicals for converting CO and CO_2, unless the ratio of molecular number densities $[SO_3]/[OH] \gg 10^7$–10^9 in the gas phase.

In fact, Fegley *et al.* (1995) observed the formation of hematite in their pyrite decomposition experiments done in CO–CO_2–SO_2 gas mixtures. The gas mixtures had approximately the same SO_2 number density and about a 10 times higher CO number density than at the surface of Venus. Hematite formation in these experiments indicates that the equilibration of CO and CO_2 is apparently not catalyzed by sulfur oxide chemistry, at least under the laboratory conditions (~390–530°C, 1 atm., 1.9% CO, 1.8% SO_2, 96.3% CO_2).

Finally, we note that our proposed kinetic inhibition model also explains why the CONTRAST experiment on the Venera 13/14 landers indicated redox conditions inside the magnetite stability field, while the color imaging from the same spacecraft indicated the presence of hematite. The reason is that the CONTRAST experiment measured the concentration of CO from its reaction with vanadium oxides, which Florensky *et al.* (1983) state is a rapid process occurring within minutes. In contrast, the color imaging measured the oxidation state of Fe minerals that are reacting with the overlying atmosphere. Even though ~10 ppm CO may be present, as indicated by the CONTRAST experiment, the slow reaction between CO and CO_2 under the anhydrous conditions at the surface of Venus will lead to an oxygen fugacity significantly higher than the predicted equilibrium value. Thus, the two experiments can indicate both a high CO concentration and a high oxygen fugacity, without necessarily contradicting each other.

SUMMARY

Hematite and other Fe^{3+}-bearing minerals are produced by heating Fe^{2+}-bearing basalt at Venus surface temperatures in gas mixtures with CO/CO_2 ratios falling inside the magnetite stability field. Additional experiments with synthetic magnetite and CuO show that the CO–CO_2 gas mixtures do not equilibrate on laboratory time scales and have oxygen fugacities that, while extremely reducing, are still several orders of magnitude greater than expected from thermochemical equilibrium calculations. The experimental results are plausibly explained by the failure of CO–CO_2 gas mixtures to equilibrate at low temperatures under anhydrous, or nearly anhydrous, conditions. The experimental results are consistent with the suggestion by Pieters *et al.* (1986) that the reflectance properties at several Venera landing sites indicate an oxidized basaltic surface containing Fe^{3+} minerals such as hematite. Further work is now underway to constrain the rate of basalt oxidation on the surface of Venus and the conditions under which CO and CO_2 may attain thermochemical equilibrium in the lower atmosphere of Venus.

ACKNOWLEDGMENTS

We thank R. Poli from Washington University and P. Held from the Technische Hochschule, Darmstadt for their assistance and Professor E. Kankeleit of the Technische Hochschule, Darmstadt for fruitful discussions. We also acknowledge helpful reviews by E. Murad, J. L. Gooding, and M. Zolotov. This work was supported by NASA Grant NAGW-4485 and the NATO Collaborative Research Program (Grant 931476).

REFERENCES

ARMSTRONG, J. T. 1988. Quantitative analysis of silicate and oxide minerals: Comparison of Monte-Carlo, ZAF and Phi-Rho-Z procedures. *Microbeam Anal.* pp. 239–246.

BURNS, R. G. 1994. Mineral Mössbauer spectroscopy: Correlations between chemical shift and quadrupole splitting parameters. *Hyperfine Interact.* **91,** 739–745.

CHASE, M. W., JR., C. A. DAVIES, J. R. DOWNEY, JR., D. J. FRURIP, R. A. MCDONALD, AND A. N. SYVERUD 1985. *JANAF Thermochemical Tables,* 3rd ed., *J. Phys. Chem. Ref. Data* **14,** supplement no.1, Am. Chem. Soc. and Am. Inst. of Phys.

DEGRAVE, E., AND A. VAN ALBOOM 1991. Evaluation of ferrous and ferric Mössbauer fractions. *Phys. Chem. Miner.* **18,** 337–342.

EHRENBERG, K. H., G. HENTSCHEL, W. SCHRICKE, AND G. STRECKER 1982. Vogelsberg-Vulkanismus. *Fortschr. Miner.* **60,** 17–42.

FEGLEY, B., JR., G. KLINGELHÖFER, R. A. BRACKETT, AND N. IZENBERG 1994a. The oxidation state of the surface of Venus. *Meteoritics* **29,** 465–466.

FEGLEY, B., JR., G. KLINGELHÖFER, AND K. LODDERS 1994b. The formation of hematite on the surface of Venus. *Bull. Am. Astron. Soc.* **26,** 1145.

FEGLEY, B., JR., K. LODDERS, A. H. TREIMAN, AND G. KLINGELHÖFER 1995. The rate of pyrite decomposition on the surface of Venus. *Icarus* **115,** 159–180.

FEGLEY, B., JR., AND R. G. PRINN 1989. Estimation of the rate of volcanism on Venus from reaction rate measurements. *Nature* **337,** 55–58.

FEGLEY, B., JR., AND A. H. TREIMAN 1992. Chemistry of atmosphere–surface interactions on Venus and Mars. In *Venus and Mars: Atmospheres, Ionospheres, and Solar Wind Interactions* (J. G. Luhmann, M. Tatrallyay, and R. O. Pepin, Eds.), pp. 7–71, Am. Geophys. Union, Washington, DC.

FEGLEY, B., JR., A. H. TREIMAN, AND V. L. SHARPTON 1992. Venus surface mineralogy: Observational and theoretical constraints. *Proc. Lunar Planet. Sci. Conf. 22nd,* 3–20.

FLORENSKY, C. P., O. V. NIKOLAEVA, V. P. VOLKOV, A. F. KUDRYASHOVA, A. A. PRONIN, YU. M. GEEKTIN, E. A. TCHAIKINA, AND A. S. BASHKOROVA 1983. Redox indicator "CONTRAST" on the surface of Venus. *Lunar Planet. Sci.* **XIV,** 203–204.

GEL'MAN, B. G., V. G. ZOLOTUKHIN, N. I. LAMONOV, B. V. LEVCHUK, A. N. LIPATOV, L. M. MUKHIN, D. F. NENAROKOV, V. A. ROTIN, AND B. P. OKHOTNIKOV 1979. Analysis of chemical composition of Venus atmosphere by gas chromatography on Venera 12. *Cosmic Res. Engl. Transl.* **17,** 585–589.

GOLOVIN, YU. M., B. YE. MOSHKIN, AND A. P. EKONOMOV 1983. Some optical properties of the Venus surface. In *Venus* (D. M. Hunten, L. Colin, and V. I. Moroz, Eds.), pp. 131–136, Univ. of Arizona Press, Tucson.

HEAD, J. W., L. S. CRUMPLER, J. C. AUBELE, J. E. GUEST, AND R. S. SAUNDERS 1992. Venus volcanism: Classification of volcanic features and structures, associations, and global distribution from Magellan data. *J. Geophys. Res.* **97,** 13,153–13,197.

HEMINGWAY, B. S. 1990. Thermodynamic properties of bunsenite, NiO, magnetite, Fe_3O_4, and hematite, Fe_2O_3, with select comments on selected oxygen buffer reactions. *Am. Mineral.* **75,** 781–790.

HUEBNER, J. S. 1975. Oxygen fugacity values of furnace gas mixtures. *Am. Mineral.* **60,** 815–823.

KANKELEIT, E. 1964. Velocity spectrometer for Mössbauer experiments. *Rev. Sci. Instrum.* **35,** 194–197.

KANKELEIT, E. 1975. Some technical developments in Mössbauer spectroscopy. In "*Proceedings, International Conference on Mössbauer Spectroscopy*" (A. Z. Hrynkiewicz and J. A. Sawicki, Eds.), Vol. 2, pp. 43–58. Krakow, Poland.

KANKELEIT, E., J. FOH, P. HELD, G. KLINGELHÖFER, AND R. TEUCHER 1994. A Mössbauer experiment on Mars. *Hyperfine Interact.* **90,** 107–120.

KARGEL, J. S., G. KOMATSU, V. R. BAKER, AND R. G. STROM 1993. The volcanology of Venera and VEGA landing sites and the geochemistry of Venus. *Icarus* **103,** 253–275.

KLINGELHÖFER, G., P. HELD, R. TEUCHER, F. SCHLICHTING, J. FOH, AND E. KANKELEIT 1995. Mössbauer spectroscopy in space. *Hyperfine Interact.* **95,** 305–339.

KRASNOPOLSKY, V. A., AND J. B. POLLACK 1994. H_2O–H_2SO_4 system in Venus' clouds and OCS, CO, and H_2SO_4 profiles in Venus' troposphere. *Icarus* **109,** 58–78.

KREUZER, H., K. KUNZ, P. MÜLLER, E. SCHENK, W. HARRE, AND H. RASCHKA 1974. Petrologie und Kalium/Argon-Daten einiger Basalte aus der Bohrung 31, Rainrod I (Vogelsberg). *Geol. Jahrb.* **9,** 67–84.

KÜNDIG, W., H. BOMMEL, G. CONSTABARIS, AND R. H. LINDQUIST 1966. Some properties of supported small Fe_2O_3 particles determined with the Mössbauer effect. *Phys. Rev.* **142,** 327–333.

LEWIS, J. S. 1970. Venus: Atmospheric and lithospheric composition. *Earth Planet. Sci. Lett.* **10,** 73–80.

LODDERS, K. 1991. Spurenelementverteilung zwischen Sulfid und Silikatschmelze und kosmochemische Anwendungen. Ph.D. thesis, Johannes Gutenberg Universität, Mainz, Germany.

MALLARD, W. G., F. WESTLEY, J. T. HERRON, AND R. F. HAMPSON 1994. *NIST Chemical Kinetics Database*—Ver. 6.0, NIST Standard Reference Data, Gaithersburg, MD.

MAROV, M. YA., V. P. VOLKOV, YU. A. SURKOV, AND M. L. RYVKIN 1989. Lower atmosphere. In *The Planet Venus: Atmosphere, Surface, Interior Structure* (V. L. Barsukov and V. P. Volkov, Eds.), pp. 25–67, Nauka, Moscow, USSR.

MCELROY, M. B., AND T. M. DONAHUE 1972. Stability of the martian atmosphere. *Science* **177,** 986–988.

MEISEL, W., P. GRIESBACH, H. J. GRABKE, AND P. GUETLICH 1990. Quantitative determination of fayalite layers on iron by CEMS. *Hyperfine Interact.* **57,** 2001–2008.

MITRA, S. 1992. *Applied Mössbauer Spectroscopy.* Pergamon Press, New York.

MORRIS, R. V., D. G. AGRESTI, H. V. LAUER, JR., J. A. NEWCOMB, T. D. SHELFER, AND A. V. MURALI 1989. Evidence for pigmentary hematite on Mars based on optical, magnetic, and Mössbauer studies of superparamagnetic (nanocrystalline) hematite. *J. Geophys. Res.* **94,** 2760–2778.

MORRIS, R. V., D. G. SCHULZE, H. V. LAUER, JR., D. G. AGRESTI, AND T. D. SHELFER 1992. Reflectivity (visible and near IR), Mössbauer, static magnetic, and X-ray diffraction properties of aluminum substituted hematites. *J. Geophys. Res.* **97,** 10,257–10,266.

MUELLER, R. F. 1964. A chemical model for the lower atmosphere of Venus. *Icarus* **3,** 285–298.

MURAD, E., AND J. H. JOHNSTON 1987. Iron oxides and oxyhydroxides. In *Mössbauer Spectroscopy Applied to Inorganic Chemistry* (G. J. Long, Ed.), Vol. 2, pp. 507–582, Plenum, New York.

PARKINSON, T. M., AND D. M. HUNTEN 1972. Spectroscopy and aeronomy of O_2 on Mars. *J. Atmos. Sci.* **29,** 1380–1390.

PIETERS, C. M., J. W. HEAD, W. PATTERSON, S. PRATT, J. GARVIN, V. L. BARSUKOV, A. T. BASILEVSKY, I. L. KHODAKOVSKY, A. S. SELIVANOV, A. S. PANFILOV, YU. M. GEKTIN, AND Y. M. NARAYEVA 1986. The color of the surface of Venus. *Science* **234,** 1379–1383.

POLLACK, J. B., B. DALTON, D. H. GRINSPOON, R. B. WATTSON, R.

FREEDMAN, D. CRISP, D. A. ALLEN, B. BÉZARD, C. DEBERGH, L. GIVER, Q. MA, AND R. TIPPING 1993. Near-infrared light from Venus' night-side: A spectroscopic analysis. *Icarus* **103,** 1–42.

PRINN, R. G. 1985. The photochemistry of the atmosphere of Venus. In The Photochemistry of Atmospheres (J. S. Levine, Ed.), pp. 281–336. Academic Press, New York.

SAWATZKY, G. A., J. M. D. COEY, AND A. H. MORRISH 1969. Mössbauer study of electron hopping in the octahedral sites of Fe_3O_4. *J. Appl. Phys.* **40,** 1402–1403.

STRAUB, D. W., AND R. G. BURNS 1991. Degradation of Fe–Mg silicates in hot CO_2 atmospheres: Applications to Venus. *Lunar Planet. Sci.* **XXII,** 1349–1350.

VAN DER KRAAN, A. M. 1973. Mössbauer effect studies of surface ions of ultrafine α-FeOOH particles. *Phys. Status Solidi A* **15,** 215–226.

VON ZAHN, U., S. KUMAR, H. NIEMANN, AND R. G. PRINN 1983. Composition of the atmosphere of Venus. In *Venus* (D. M. Hunten, L. Colin, T. M. Donahue, and V. I. Moroz, Eds.), pp. 299–430. Univ. of Arizona Press, Tucson.

WARNATZ, J. 1984. Rate coefficients in the C/H/O system. In *Combustion Chemistry* (W. C. Gardiner, Jr., Ed.), pp. 197–360, Springer-Verlag, New York.

YUNG, Y. L., AND W. B. DEMORE 1982. Photochemistry of the stratosphere of Venus: Implications for atmospheric evolution. *Icarus* **51,** 199–247.